IEEE Access
Multidisciplinary | Rapid Review | Open Access Journal

Received October 25, 2019, accepted November 13, 2019, date of publication November 18, 2019,
date of current version December 2, 2019.

Digital Object Identifier 10.1109/ACCESS.2019.2953979

Feedback Timing Method Based on Joint Optimization Function of Code Period and Timing Parameters in Non-Cooperative Communication

YOUYANG LI[1,2], FEI QIN[1,3], (Member, IEEE), XUE WANG[1,2], AND XIAOCHUN LU[1,2]

[1]School of Electronic, Electrical and Communication Engineering, University of Chinese Academy of Sciences, Beijing 100049, China
[2]National Time Service Center, Chinese Academy of Sciences, Xi'an 710600, China
[3]Key Laboratory of Information Technology for Autonomous Underwater Vehicles, Chinese Academy of Sciences, Beijing 100190, China

Corresponding author: Xue Wang (wangxue@ntsc.ac.cn)

This work was supported in part by the Scientific Instrument Developing Project of the Chinese Academy of Sciences under Grant YJKYYQ20170074, and in part by the Open Project of Key Laboratory of Information Technology for Autonomous Underwater Vehicles, Chinese Academy of Sciences.

ABSTRACT In non-cooperative communication, the code frequency, the pulse shaping filter and other prior parameters are unknown to the receiver, which increases the challenge of non-cooperative receiving system design. A straightforward method may estimate these parameters in advance following traditional receiving systems. Estimation errors will undoubtedly be involved and passed between stages, which will decease system performance, especially in low signal-to-noise ratio (SNR) scenarios. To address this problem, this paper constructs a carefully designed optimization function for timing estimation that combines both the code frequencies and the timing parameters from multiple chips. Consequently, a feedback-based tracking model is proposed to solve such an optimization function. Finally, extensive simulation results validate the efficiency of the proposed method, which achieves ten times better accuracy than the traditional method and can partially overcome the influence of code frequency deviations.

INDEX TERMS Non-cooperative communication, timing estimation, Gardner detector, self-noise, early-late detector, code loop tracking.

I. INTRODUCTION

In military communications, it is essential to obtain information from or effectively interfere with enemy communications. To achieve these goals, a receiver must detect signals, estimate their unknown parameters and accurately demonstrate the results. Similarly, in civil communications, to ensure the effective use of spectrum resources, communication regulators usually need to confirm legitimate communications and monitor illegal communications, which also require the capability to detect and estimate unknown received signals. This type of unauthorized receiver usually uses modern signal processing methods to obtain effective information from the captured signals. Usually, this type of receiver will not affect the normal communication of primary users. As a result, this type of communication is usually known as ''non-cooperative communication'' [1]. For convenience of discussion, the target signal involved in the following discussion will be referred to as a ''non-cooperative signal''. The corresponding process of demodulating non-cooperative signals in non-cooperative communication is known as ''blind demodulation'' [2]. In a typical cooperative communication process, communication devices usually exchange a priori information on the communication mode using handshake protocols. Received data signals can be demodulated by directly using the prior parameters of the current communication mode. However, in non-cooperative communication, devices attempt to receive and demodulate intercepted signals without the required information. Therefore, the prior information needs to be estimated to perform demodulation and other subsequent operations. This process is known as non-cooperative communication in this paper.

As shown in Fig.1, the jump points between chips are not obvious for baseband signals even after carrier stripping due to the influence of shaping filtering. Inaccurate estimation of

The associate editor coordinating the review of this manuscript and approving it for publication was Wu-Shiung Feng.

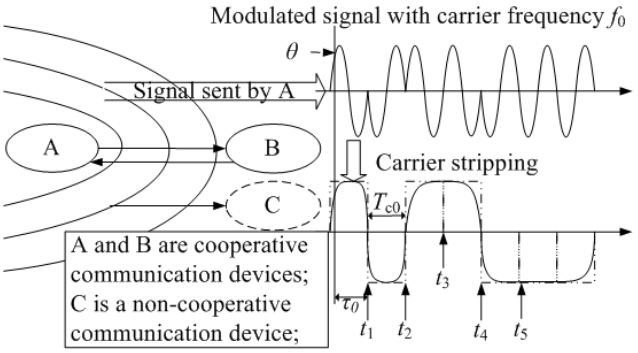

FIGURE 1. Non-cooperative communication schematic.

the jump points can result in symbol aliasing and introduce intersymbol interference (ISI), thus increasing the bit error rate (BER). As a result, accurate timing parameters and the code period must be known to segment the complete symbol period. This is because higher demodulation performance can only be achieved with accurate segmentation of the symbol period. Nonetheless, accurate timing estimation is obviously one of the most important algorithms in non-cooperative communication.

For scenarios with continuous incoming signals, iterative timing methods based on continuous time segment data are widely utilized and are known as feedback timing, e.g., the Gardner (GAD) method [9] and the early-late method [10], [11]. This type of method uses the results from the previous cycle for iterative estimation and offers higher estimation accuracy with less computation. It should be noted that the existing back-feedback methods are mainly used for timing tracking of cooperative signals with known prior parameters. For example, some methods require accurate code period parameters [8], use the pulse shaping filter function [14], or rely on other prior information [15]. For non-cooperative communication, this prior parameter information is usually unknown, and estimating this information can further increase the estimation error. Moreover, if the system works in a low signal-to-noise (SNR) ratio, the estimation of these prior parameters will introduce more self-noise, leading to significant timing deviations. Similarly, if the shaping filter coefficient or the code period is inaccurate, the self-noise variance [7] will also be increased and lead to a final timing deviation [23].

This paper works with a baseband signal down-converted from a carrier frequency. A novel direct feedback-based timing estimation algorithm is proposed to reduce the influence of self-noise and channel noise over chip cycles, where a joint optimization function with both code periods and timing parameters is carefully designed to avoid the problems mentioned in traditional algorithms. A loop filter process has been proposed to iteratively solve the optimization function, where the timing parameter and the code period parameter will converge to the optimal value. The main contribution of the algorithm proposed in this paper can be summarized as follows:

(1) This paper theoretically analyzed the timing problem with limited prior information, revealing the essential reasons why existing methods suffer poor performance in this scenario.

(2) This paper proposed an integral-based optimization function that further involves the code frequency to resist the effect of both noise and frequency deviation.

(3) This paper implemented a loop filtering-based algorithm to approach the optimized solution with low complexity and high accuracy, which have been validated by extensive simulations.

This paper is organized as follows: Section II introduces the mathematical model of the modulated signal and the feedback timing framework. Section III introduces the early-late-PI feedback timing method for the joint code period proposed in this paper. In Section IV, the performance and estimation accuracy of the proposed algorithm are validated by numerical experiments. The section V summarizes the work and contribution in this paper.

II. SYSTEM MODEL

As shown in Fig. 1, if a linear modulated signal (e.g., PAM, M-QAM, M-PSK, etc.) is transmitted by user A, the signal model $s(t)$ can be written as:

$$s(t) = \sum_{i=0}^{N_0-1} e^{j(\theta+2\pi f_0 t)} a_i g(t - iT_{c0} - \tau_0) + w(t), \quad (1)$$

where θ is the initial carrier phase, f_0 is the carrier frequency, a_i is the transmitted data symbol sequence which is assumed to be independent and identically distributed, $g(t)$ is the impulse response of the transmission filter, $w(t)$ is complex Gaussian white noise, T_{c0} represents the code period and τ_0 is the timing parameter. The following baseband signals can then be obtained after carrier synchronization and carrier stripping:

$$s_L(t) = \sum_{i=0}^{N_0-1} a_i g(t - iT_{c0} - \tau_0) + w_b(t). \quad (2)$$

Taking the baseband signal in Fig.1 as an example, if the timing parameter $\hat{\tau}_0$ and the code period $\hat{T}_{c0}$ can be accurately estimated, then the position $t_i = \hat{\tau}_0 + (i-1)\hat{T}_{c0}$ of each hopping node can thus be calculated. Thereafter, the timing information can be used as a benchmark to extract the symbol slices (i.e., the sampling sequence between t_i and t_{i+1}) and to execute the following judgment: if the signal is BPSK, then if $\int_{t_i}^{t_{i+1}} s_L(t)\,dt > 0$, a_i is judged to be symbol "1", otherwise a_i is symbol "-1". Obviously, the more accurate the timing parameter $\hat{\tau}_0$ and the code period $\hat{T}_{c0}$ are, the higher the detection probability of symbol sequence $\{a_i\}$ will be.

Solving for the timing parameter usually requires a feedback timing framework [8], [12], [16], [22], [24], as shown in Fig.2. In this figure, the "TED parameter acquisition" block is used to acquire parameters, which must be calculated before the timing error detector (TED). The classic solutions include the resampling process (interpolator) of the GAD

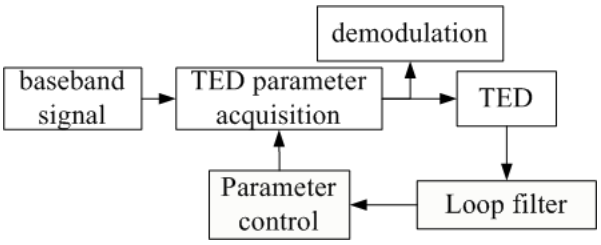

FIGURE 2. Flow chart of feedback timing framework.

method [9] and the correlation integration (integrator) process [12] widely utilized in the spread spectrum code tracking system. The ''Parameter control'' block is used to obtain the timing parameters for the current time and provides input into the ''TED parameter acquisition'' block.

III. TIMING TRACKING MODEL BASED ON THE JOINT OPTIMIZATION FUNCTION

A. PROPOSED JOINT OPTIMIZATION FUNCTION

Traditional feedback timing methods [8]–[11], [13]–[24] can be regarded as theoretical processes used to determine the optimal solution of an optimization function. For a non-spread spectrum linear modulation signal timing process, the maximum value of the shaping filter function $g(\tau)$ must be obtained. The solving process is also constrained by the stabilization of each resampling point $y(t_{k+0.5})$ at its maximum point. Different methods have been utilized for different TED constructions. For example, the GAD method [9] utilizes the feedback iteration $(y(t_{k+1}) - y(t_k))\, y(t_{k+0.5})$, where $y(t_{k+1})$ represents the resampling point at $t_{k+0.5} + 0.5T_{c0}$, and $y(t_k)$ is the resampling point at $t_{k+0.5} - 0.5T_{c0}$. The early-late method [19] uses the feedback iteration $y^2(t_{k+0.5} + DT_{c0}) - y^2(t_{k+0.5} - DT_{c0})$, where D represents the early-late chip period ratio. For a spread-spectrum signal timing process, the optimization function works with the cross-correlation function $R(\tau)$ of the spread-spectrum sequence. As a result, spread spectrum signals usually have good anti-noise performance through the correlation integral. For the tracking of non-spread spectrum signals, the correlation gain through the integral can also be expected with match filtering with essentially the same approach. Then, one can hypothesize that the timing performance can be improved by involving the integral into the optimization function by translating and stretching the integration window as shown in Fig.3. It should also be noted that the optimization function of the existing methods usually fails to consider the inaccuracy of code frequency, which motivated this paper to construct a joint optimization function and introducing the code period into the optimization function at the same time.

After the time delay τ, the integral in the k-th integration window is expressed as $\int_{\tau+k\cdot T_c}^{\tau+(k+1)\cdot T_c} s_L(t)\, W(t, f_c, \tau)\, dt$. The weighted signal $s_L(t)$ is integrated in the interval $[\tau + k \cdot T_c \tau + (k+1) \cdot T_c]$, where $W(t, f_c, \tau)$ is a weighted function. As shown in Fig.3, the timing parameter τ controls the position of the window, and the code period T_c controls

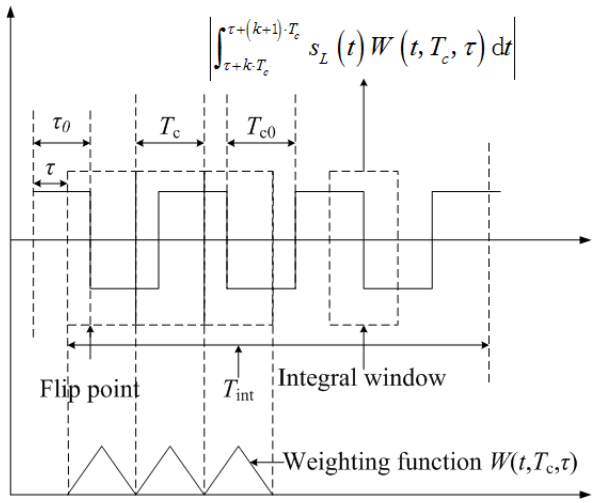

FIGURE 3. Explanation diagram of the optimized function.

the width of the integration window. Then, the translation is controlled by τ, and the window stretching is controlled by T_c. Finally, the optimization can reach the maximum value if each integration window is aligned with the target signal, i.e., each window can integrate a complete chip. The results of the piecewise integration in the T_{int} period can be divided into two outcomes. The first is the integral resulting in a complete integral window. The absolute value is obtained after the determining the integral in N_c complete integral windows. Then, the integral sum is obtained: $\sum_{k=0}^{N_c-1} \left|\int_{\tau+k\cdot T_c}^{\tau+(k+1)\cdot T_c} s_L(t)\, W(t, f_c, \tau)\, dt\right|$. The second outcome is the integral resulting in a remaining incomplete integral window. The absolute value for the integral within $[\tau + N_c \cdot T_c, T_{int}]$ is $\left|\int_{\tau+N_c\cdot T_c}^{T_{int}} s_L(t)\, W(t, f_c, \tau)\, dt\right|$. Then, the optimization function $J(T_c, \tau)$ can be expressed as follows (hereinafter referred to as the J function):

$$J(T_c, \tau) \triangleq \sum_{k=0}^{N_c-1} \left|\int_{\tau+k\cdot T_c}^{\tau+(k+1)\cdot T_c} s_L(t)\, W(t, f_c, \tau)\, dt\right| + \left|\int_{(\tau+N_c)\cdot T_c}^{T_{int}} s_L(t)\, W(t, f_c, \tau)\, dt\right|, \quad (3)$$

where $|\tau| < T_c$, $T_c < T_{int}$, $N_c = fix\left(\frac{T_{int}-\tau}{T_c}\right)$, T_{int} represents the total time of the acquisition signal, and $fix(\cdot)$ is a function of the integral to zero. The proposed optimization function is then established using the relationship between the integrated received baseband signal within the integration window decided by the delay time τ and code period T_c.

If it is assumed that if the directions of any two adjacent chips are different (i.e., the chip information is 010101...), then the chip waveform is an ideal square wave chip, as shown in Fig.3. (a) It is assumed that if $T_c = T_{c0}$, the width of the integration window is exactly equal to the width of the chip. Then, if the edge of the integration window is exactly in the middle of the chip after delaying τ, it will be equal to zero for every integration window in T_{int}. The optimization

function reaches a minimum value after summing all the integration windows. If the edge of the integration window is accidentally located in a position where the chip edge flips after a delay, then each integration window contains a complete chip period. As a result, the absolute value of integration in the integration window will reach its maximum value. Specifically, the integral value will reach its maximum value within time T_{int}. (b) When the first integral window is aligned (i.e., the timing parameter τ is accurate $\tau = \tau_0$ and the edge of the first integral window is just at the edge of the chip) and T_c is deviated from the real code period T_{c0} of the signal, the offset between the edge of each subsequent integral window and the chip flip point will be accumulated during the derivation. The output value of the optimization function will deviate from the maximum value after summing the absolute value of the piecewise integration. Combining the analyses of (a) and (b), i.e., $(T_c = T_{c0}, \tau = \tau_0)$ provides the location of the maximum of this optimization function. The precise timing parameters and code period can be obtained by solving the joint optimal solution problem:

$$\left[\hat{T}_{c0}, \hat{\tau}_0\right] = \underset{T_c,\tau}{argmax}\, J\left(T_c, \tau\right). \tag{4}$$

Due to the influence of sampling, the peak of the optimization function will be ladder-like without a weighted function $W\left(t, T_c, \tau\right)$, as shown in Fig.7 (a). This will cause $1/Q$ ambiguity (Q represents oversampling rate) at the zero-crossing point of the S curve, and lead to fluctuations in the loop feedback phase within $1/Q$. To solve this problem, a weighting function $W\left(t, T_c, \tau\right)$ is constructed. The purpose of the weighting function is similar to that of the interpolation function in the GAD method and provides high-precision TED feedback at a low sampling rate, without limiting the sampling rate. The expression of the weighted function is shown in (5):

$$\begin{aligned} W\left(t, T_c, \tau\right) = &\left(1 - W_0\left(t, T_c, \tau\right)\right) a_1\left(t, T_c, \tau\right) \\ &+ W_0\left(t, T_c, \tau\right) a_2\left(t, T_c, \tau\right), \end{aligned} \tag{5}$$

where

$$\begin{cases} W_0\left(t, T_c, \tau\right) = \mathrm{mod}\left(t \cdot T_c + \tau, 1\right) \\ a_1\left(t, T_c, \tau\right) = W_0\left(t, T_c, \tau\right) > 0.5 \\ a_2\left(t, T_c, \tau\right) = \left|1 - a_1\left(t, T_c, \tau\right)\right|, \end{cases} \tag{6}$$

$W_0\left(t, T_c, \tau\right) > 0.5$ means that if $W_0\left(t, T_c, \tau\right)$ is greater than 0.5 at time t for a given value of T_c and τ, it will be made equal to one, otherwise it is zero.

As shown in Fig.4, it is assumed that the baseband signal is an ideal square wave signal with an amplitude equal to 1 and an oversampling rate equal to 4, and where the abscissa number equals a multiple of the code period. For example, the first sampling point is $0.125T_{c0}$, and the interception point is $0.5T_{c0}$, and the timing parameter for the interception point is $\tau = 0$. In this case, if there is no weighting function, the results calculated by the J function at $\tau = -0.1T_{c0}$ and $\tau = -0.2T_{c0}$ are the same. When $\tau = -0.2T_{c0}$,

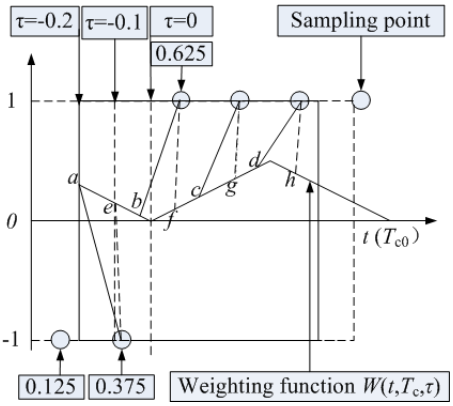

FIGURE 4. Weighted function description graph.

the magnitude of the weighted function after sampling will be $[a, b, c, d]$ and the weighted sum in the integral window is $J\left(T_{c0}, -0.2T_{c0}\right) = b + c + d - a$. When $\tau = -0.2T_{c0}$, the magnitude of the weighted function $W\left(t, T_c, \tau\right)$ after sampling will be $[e, f, g, h]$ and the weighted sum in the integral window is $J\left(T_{c0}, -0.1T_{c0}\right) = f + g + h - e$. If $b + d = f + h$, it is obvious that $c - a < g - e$ so $J\left(T_{c0}, -0.1T_{c0}\right) > J\left(T_{c0}, -0.2T_{c0}\right)$ and the weighting function will ensure that the output of the J function is continuous (rather than suddenly jumping without the weighting function), which is similar to the effect of the interpolation function. The specific contrast effect will be discussed in further detail later in the numerical experiment.

B. SOLUTION OF LOOP FILTER FOR OPTIMIZED FUNCTION

In this paper, the optimization model is solved following the similar method of the code loop tracking process in navigation signals [24]. Since the navigation signal is a type of spread spectrum signal with a large bandwidth, the spread spectrum code frequency is very high and is sensitive to Doppler effects. Therefore, the code period is also considered a variable for loop tracking. As the situation in this paper is similar to the above situation, the optimization function designed in the last section may be solvable with a similar approach. In addition, a navigation signal can generate its local spread spectrum code during the tracking process, which will be multiplied by the received signal by its shift and then integrated over the output $R\left(\tau, T_c\right)$. For a non-cooperative signal, the output should be calculated using the J function with feedback obtained by the TED. Therefore, the values of T_c and τ after loop filtering (as shown in Fig.5) are submitted into the J function of formula (5). The calculation process is equivalent to the correlation integral role in the spread spectrum signal tracking process.

The loop filter model in Fig.5 is composed of three parts. The first part, the J function calculation process, is shown within the dashed line frame and corresponds to the integration process used in navigation signal tracking. The second part, the "TED" process, corresponds to the code loop discriminator process in the navigation signal described on

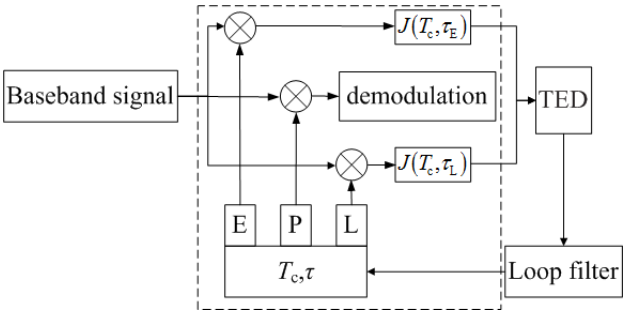

FIGURE 5. Feedback timing block diagram of early-late-PI method.

pg. 174 in [12]. The parameter D represents the code phase spacing in the advance and delay reduction (as defined on pg. 194 in [12]). The third part, the "Loop filter" process, may vary in orders depending on the system design. The parameters for the loop filter include the damping coefficient ξ and the characteristic frequency ω_n. The stability of the loop filter has been proven in [3].

As shown in Fig.7, the waveform of the J function in the τ domain is similar to that of the correlation function $R(\tau, T_c)$ in the τ domain, and it has symmetrical characteristics. Therefore, reference can be made directly to the code loop discriminator model pg. 174 [12] for the navigation signal. This paper employs the $\frac{E-L}{E+L}$ code loop discriminator method as the TED for feedback timing.

In Fig.5, module "P" indicates the timing parameter τ_P and the code period parameter τ_P of the loop filter output at the current time which are used for demodulation. In module "E", $\tau_E = \tau_P + \frac{D}{2}T_c$ is obtained by adding future time $\frac{D}{2}T_c$ to the current timing parameter τ_P. In module "L", the current timing parameter τ_P is subtracted from the lag time $\frac{D}{2}T_c$ to obtain $\tau_L = \tau_P - \frac{D}{2}T_c$. The code periods T_c, τ_E and τ_L are entered into the J function to obtain $J(T_c, \varepsilon_E)$ and $J(T_c, \varepsilon_L)$. The TED expression in this paper can be obtained using the $\frac{E-L}{E+L}$ code loop discrimination method as follows:

$$e_p = \frac{J(T_c, \varepsilon_E) - J(T_c, \varepsilon_L)}{J(T_c, \varepsilon_E) + J(T_c, \varepsilon_L)}, \tag{7}$$

where e_p represents the result of the TED output at the current time.

To facilitate a discussion and comparison of the methods, the following parameter transformations will be carried out: The code period parameters are transformed into code frequency $f_c = 1/T_c$, and the timing parameters are normalized to $\varepsilon = \tau/T_c$, where ε is the normalized code phase and can be expressed as:

$$J(T_c, \tau) \to J(f_c, \varepsilon T_c) \to J(f_c, \varepsilon). \tag{8}$$

By combining formulas (7) and (8), the output of the k-th TED in signal tracking can be expressed as follows:

$$e_p(k) = \frac{J(f_c(k), \varepsilon_E(k-1)) - J(f_c(k), \varepsilon_L(k-1))}{J(f_c(k), \varepsilon_E(k-1)) + J(f_c(k), \varepsilon_L(k-1))}. \tag{9}$$

Then, in the process of loop filtering, the updating process of code frequency $f_c(k)$ and normalized code phase $\varepsilon_p(k)$ is

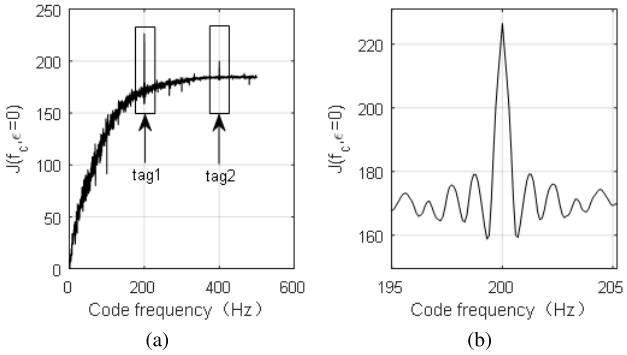

FIGURE 6. Code frequency domain properties of optimal functions. (a) Overall frequency domain curve; (b) Amplification frequency domain curve at f_{c0}.

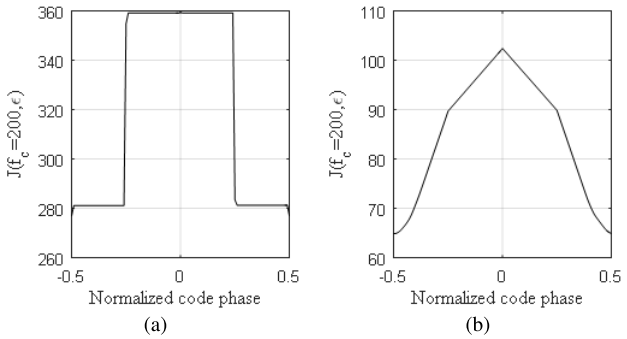

FIGURE 7. Phase domain properties of normalized codes for optimized functions. (a) Optimal function without W-weighted function; (b) Optimal function with W-weighted function.

as follows:

$$\begin{cases} r_c(k) = r_c(k-1) + K_1 \cdot e_p(k) \\ f_c(k) = f_{ci} + K_2 \cdot e_p(k) + r_c(k) \\ \varepsilon_p(k) = f_c(k) \cdot T_{int} + \varepsilon_p(k-1). \end{cases} \tag{10}$$

where f_{ci} is the initial code frequency, K_1 and K_2 are filter coefficients, and the relationship between the characteristic frequency ω_n and the damping coefficient ξ is $K_1 = \omega_n^2 \cdot T_{int}$, $K_2 = 2\omega_n \cdot \xi$. The convergence and accuracy of the system will be demonstrated in the next section through numerical simulation experiments.

IV. SIMULATION-BASED EXPERIMENTAL RESULTS

The method described in [8] is chosen in this paper (hereinafter referred to as M-GAD) as the baseline for comparison; since this paper uses a data averaging method for multiple chip periods to reduce self-noise interference, this method can effectively reduce the influence of external white noise and is thus very suitable for the application in this paper.

A. PROPERTY OF OPTIMAL FUNCTION

The characteristics of the J function for the dimensions of the two variables are shown by numerical experiments. Fig.6 is the fluctuation curve of the J function over the f_c interval [0, 500] Hz in the code frequency domain, i.e., the change in $J(f_c, \varepsilon = \varepsilon_0)$. Fig.7 shows the fluctuation curve of the

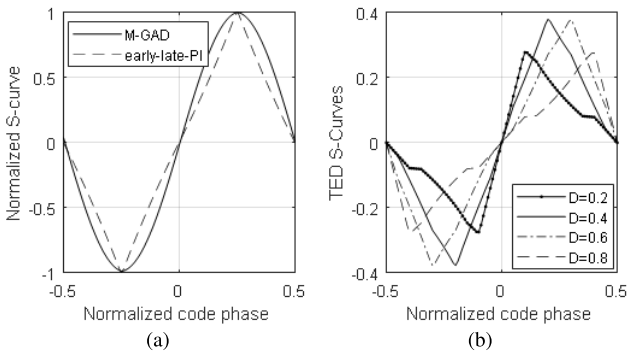

FIGURE 8. S-curve comparison of TED. (a) S curve of the early-late-PI method is compared with that of the M-GAD method; (b) S-Curve of the Early-late-PI method for different code phase spacing values.

normalized code phase over the interval $[-0.5, 0.5]$, i.e., the change in $J\ (f_c = 1/T_{c0}, \varepsilon)$. For this simulation, the oversampling rate is 4, the code frequency is 200 Hz, the roll-off coefficient is 0.3, and the integration time is $T_{int} = 1$ s.

From the analysis in Section III-A, i.e., constructing the optimization function, it is easy to notice that if the integration window is aligned with the chip flip point, any integer multiple of the integration window can also cover a single chip completely. In this case, there will be an extreme at position $T_c = T_{c0}/n$ (where n is a positive integer that is converted to position $f_c = nf_{c0}\,(f_{c0} = 1/T_{c0})$ in the code frequency domain). In Fig.6 (a), ''tag1'' shows the position where the code frequency $f_c = f_{c0}$ and ''tag2'' shows the position where the code frequency $f_c = 2f_{c0}$.

For the actual loop tracking process, the initial code frequency (similar to the acquisition process in navigation signals) is obtained using the code frequency estimation method [20], [21], and should be within the peak width shown in Fig.6 (b). It has been theoretically proven (as shown in the Appendix) that the width of the peak is approximately $1/T_{int}$. Therefore, the initial code frequency estimation accuracy should be maintained below $1/2T_{int}$ to ensure that the method described in this paper can converge. The numerical results in Fig.7 demonstrate the effectiveness of the weighting function, as the signal peak can be seen to be sharper and more continuous.

B. TED PROPERTIES

The S-curve of the TED reflects the timing accuracy to some extent, and thus several numerical experiments are shown in this section. Fig.8 (a) shows a comparison between the S-curve of the early-late-PI method and the S-curve of M-GAD when the correlator interval is 0.5. Fig.8 (b) shows a comparison of the S-curve of the early-late-PI method for different correlator intervals.

The zero-crossing slope of the S-curve reflects the accuracy of the TED, i.e., a higher zero-crossing slope correlates with a higher estimation accuracy after loop stabilization. A brief introduction of the S-curve will be provided at this point. In Fig.8 (a), the output functions of the two methods are obtained by normalizing the maximum value. At $D = 0.5$, the S-curve of the early-late-PI method is consistent with the S-curve of the M-GAD method, including the coordinates of the zero-point and the extreme point (it should be understood that the GAD method is a type of early-late method at D=0.5). Fig.8 (b) shows that the smaller the code phase spacing is, the larger the zero crossing point slope will be, which is consistent with the conclusions for the spread spectrum signal model. However, for smaller values of code phase spacing, it will be easier to lose the lock, and thus it should not be too small in practical applications.

In this paper, the code phase and code frequency can be corrected simultaneously using a delay lock loop (DLL) process and thus the accuracy of the initial code frequency is limited in the code frequency correction process. As per the proof given in the Appendix, the peak width of the code frequency domain is related to the integration time T_{int}. A longer integration time corresponds with a narrower wave peak, and thus requires a narrower bandwidth design in the loop filtering, to prevent convergence to the wrong code frequency point or divergence. For longer integration times and narrower peak values, the measurement accuracy will also be higher, but will require a higher initial code frequency estimation accuracy.

C. TIMING PERFORMANCE VERIFICATION

The performance of the proposed early-late-PI method is compared with the traditional M-GAD method by simulating the two methods tracking the same signal.

The accuracy of the algorithm is evaluated using the mean square error (MSE) of the normalized timing after the algorithm converges and stabilizes. The smaller the MSE of the timing is, the higher the explicit timing accuracy is. Since only non-cooperative signals are studied in this paper, the following three factors should be considered: 1) the signal-to-noise ratio, 2) the roll-off coefficient, and 3) the code frequency deviation. The Modified Cramer-Rao Bound (MCRB) formula [4], [5] for timing estimation based on the data from L_0 code cycles is given as follows:

$$MCRB\,(\varepsilon) = \frac{MCRB\,(\tau)}{T_c^2} = \frac{1}{8\pi^2\zeta L_0}\frac{N_0}{E_s}, \tag{11}$$

where E_s represents the signal energy, N_0 is the noise energy, ζ is related to the roll-off coefficient and is approximately given by $\zeta \approx \frac{1}{12} + \alpha^2\left(\frac{1}{4} - \frac{2}{\pi^2}\right)$ for linear modulation and α is the roll-off coefficient.

Since the loop filter in [4] is only for feedback timing of a single code period interval, it is not suitable when there are multiple code period feedback timings. In [6], the navigation signal code tracking process takes multiple chip cycles into account to derive the timing variance. Therefore, based on the estimation accuracy method for the navigation signal, the MCRB value for multiple chip feedback timing is derived in this paper as shown in formula (10):

$$\sigma_s^2 \cong \sigma_u^2 2B_L T_{int}\,(1 - 0.5B_L T_{int})\,, \tag{12}$$

TABLE 1. Parameter representation and settings.

Description of parameters	Symbolic Representation	Parameter values
Integral time	T_{int}	1 s
Natural radian frequency	ω_n	0.1 Hz
Damping coefficient	ξ	0.7
Code phase spacing	D	0.5

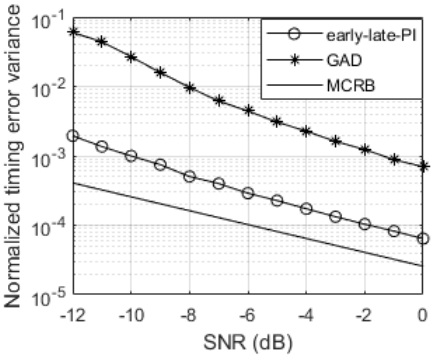

FIGURE 9. Timing accuracy at low SNR.

where σ_u^2 represents the TED output variance after stabilization, T_{int} represents the integration time or feedback time interval of the loop filter, and B_L represents the bandwidth of the loop filter. In this simulation, a first-order loop filter is used with bandwidth $B_L = \frac{\omega_n}{4}$ [7]. $\sigma_u^2 = MCRB(\varepsilon)$ can be substituted into formula (10) to obtain a value for $MCRB_{DLL}(\varepsilon)$ after the loop filter. The specific expression is as follows:

$$MCRB_{DLL}(\varepsilon) \cong \frac{1}{8\pi^2 \zeta L_0} \frac{N_0}{E_s} \cdot \frac{\omega_n}{2} T_{int} \left(1 - \frac{\omega_n}{8} T_{int}\right). \quad (13)$$

The simulated BPSK signal parameters are set as follows: the code frequency is assumed to be 200 Hz, and the oversampling rate is 4. The following three sections will discuss the influence of three factors (SNR, code frequency deviation and the shaping filter coefficient) on the estimation accuracy of the algorithm. In this simulation process, the loop filter parameters were set as shown in Table 1.

1) EFFECT OF SIGNAL-TO-NOISE RATIO (SNR)

This paper focuses on the timing method with low SNR, so the estimation accuracy of the algorithm is obtained for SNR values in the range of [−12, 0] dB. The other parameters of the signal are constant: the shaping filter coefficient is 0.9, the code frequency deviation is 0 and the oversampling rate is 4. The experimental results are shown in Fig.9.

From these estimation results, we can observe that both methods have a trend that is consistent with the MCRB trend, and the timing accuracy of the proposed early-late-PI method is ten times higher than that of the GAD method. Therefore, the method has good anti-noise performance and can achieve high estimation accuracy at a very low signal-to-noise ratio. Although the slope of the zero-crossing point of the S-curve of the M-GAD method is larger, as mentioned in section IV-B, this does not correspond with higher precision, indicating that the method proposed in this paper has better anti-noise performance for mapping the original signal to the S-curve. The product window used in the process of constructing the optimization function of this paper, described in Section III-A, is equivalent to low-pass filtering and plays a role in filtering out high-frequency noise.

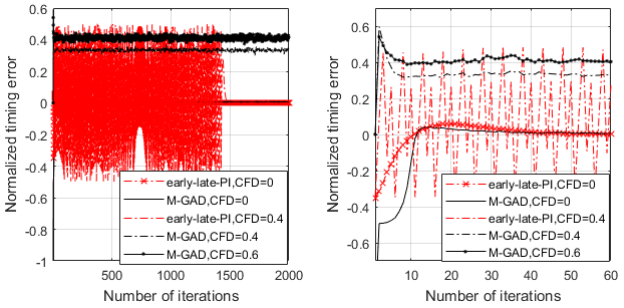

FIGURE 10. Error magnitude of normalized timing parameter in tracking process: (a) global results; (b) details of initial convergence.

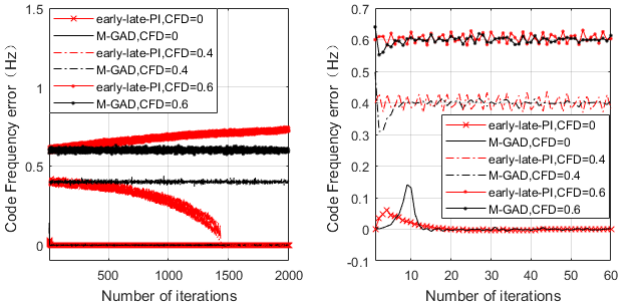

FIGURE 11. Error magnitude of the code frequency parameter in the tracking process: (a) global results; (b) details of the initial convergence.

2) EFFECT OF CODE FREQUENCY DEVIATION

In the simulation process, three code frequency deviation (CFD) values are chosen: 0 Hz, 0.4 Hz and 0.6 Hz. First, the convergence rate of the two methods is compared for CFD=0 Hz. Second, the convergence of the proposed method is verified to be bounded by the code frequency error using CFD=0.4 Hz and CFD=0.6 Hz, and the effect of the code frequency deviation on both methods is compared. The other parameters are set as follows: the roll-off factor is 0.9, and the oversampling rate is 4. To avoid the influence of noise on the statistical timing deviation, channel noise is not added for the simulation process. The convergence of the code phase is shown in Fig.10 and the convergence of the code frequency is shown in Fig.11.

When there is no code frequency deviation, i.e., CFD= 0 Hz, both methods have the same convergence speed. When CFD=0.4 Hz, the fluctuation of the "early-late-PI" method is more intense when it begins to converge. Although the proposed method may need longer iterations to converge, i.e., after 1500 iterations in the presented

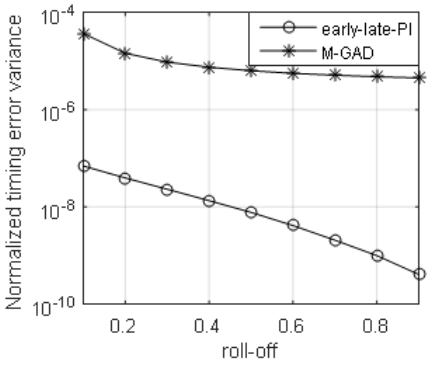

FIGURE 12. Comparison of simulation results of roll-off coefficient.

experiment, it will always gradually converge to the true value and show almost no fluctuation after the convergence. At the same time, the M-GAD method converges quickly but will suffer from not only a large estimation error but also large variations. However, when the code frequency deviation is greater than 0.5 Hz, the method in this paper will diverge, as shown the simulation result of ''early-late-PI, CFD=0.6 Hz'' in Fig.11, which is consistent with the conclusion described in Section III-B of this paper (the divergence of timing in Fig.10 is not shown because the timing parameters fluctuate within [−0.5, 0.5] in this case, which affects the display.). Although the M-GAD method does not diverge, the timing deviation caused by the code frequency deviation is large enough to prevent correct demodulation. The M-GAD method itself is based on a known code frequency and uses the symmetrical property of the chip to provide timing feedback. However, if the code frequency is uncorrected at the same time during the iteration process, it will not be able to provide correct feedback in the process of the code loop.

However, the optimization function proposed in this paper will not affect the correction of the feedback phase as long as the initial code frequency deviation is within a certain range. Consequently, the method in this paper can always converge to the correct code frequency, and the timing parameters will also converge correctly.

3) EFFECT OF ROLL-OFF COEFFICIENT

To avoid the influence of noise on the MSE trend and only focus on the effect of the roll-off coefficient, no additional white noise was added in this simulation process. The timing result error shown in Fig.12 is caused by the influence of self-noise. Self-noise is introduced based on the construction of the algorithm, so any difference in final results is due to the nature of the algorithm itself.

Fig.12 shows that the variances of both methods in timing estimation error decreases as the roll-off factor increases, i.e., as the accuracy increases. The M-GAD method has a much lower accuracy, which indicates that the shaping filtering introduces more self-noise to M-GAD. Therefore, the improved method using the GAD method [18], [22] also describes the requirement for matched filtering and forward filtering to improve the estimation accuracy. However, the method proposed in this paper is less affected by the self-noise caused by shaping filtering and can achieve high accuracy without matched filtering. As a result, the proposed method is more suitable for the non-cooperative signal scenario proposed in this paper.

V. CONCLUSION

In this paper, a novel feedback timing method known as the early-late piecewise integration method is proposed for non-cooperative signal code synchronization scenarios. Three factors (i.e. signal-to-noise ratio, code frequency deviation and shaping filter coefficient) are studied through simulation. The influence of these factors on timing accuracy is compared with the performance of the M-GAD method under the same influencing factors to validate the efficiency of proposed method. In summary, the method proposed in this paper has the following advantages: 1) higher estimation accuracy at low signal-to-noise ratio; 2) accurate convergence to the actual code frequency within certain range of code frequency deviation, ensuring that the timing estimation results will not be affected by code frequency deviations; 3) high timing accuracy for signals with even very small shaping filter coefficients, which can avoid requirements of matched filtering and forward filtering in practical applications.

APPENDIX

Although the arrangement of symbols (or changes in amplitude) in $\{a_i\}$ will affect the overall trend of $J(f_c, \tau)$ in the code frequency domain, the width of the peak near f_{c0} is the same. Therefore, the $\sin(\pi f_{c0} t + \theta_0)$ function is used as the baseband signal $s_L(t)$ to verify the peak width at f_{c0} after the J integral. For the convenience of derivation, the absolute value in formula (3) is converted to a square value. Additionally, any change in the delay τ and the weight function will not affect the peak width at f_{c0}. The J function is then transformed into the following form:

$$J(f_c, 0) \approx \sum_{i=0}^{N_c-1} \left(\int_{iT_c}^{(i+1)T_c} \sin(\pi f_{c0} t + \theta_0)\, dt \right)^2$$

where

$$\begin{aligned}
&\int_{iT_c}^{(i+1)T_c} \sin(\pi f_{c0} t + \theta_0)\, dt \\
&= \frac{-\cos(\pi f_{c0} t + \theta_0)}{\pi f_{c0}} \Bigg|_{iT_c}^{(i+1)T_c} \\
&= -\frac{1}{\pi f} \left(\cos\left[(i+1) T_c \cdot \pi f_{c0} + \theta_0\right] - \cos\left(iT_c \cdot \pi f_{c0} + \theta_0\right)\right) \\
&= \frac{2}{\pi f_{c0}} \left(\sin\left[(i+0.5) T_c \cdot \pi f_{c0} + \theta_0\right] \sin\left(\frac{T_c \cdot \pi f_{c0}}{2} \right) \right)
\end{aligned}$$

Then:

$$
\begin{aligned}
&J\left(fc,0\right)\\
&=\sum_{i=0}^{N_c-1}\left(\int_{iT_c}^{(i+1)T_c}\cos\left(\pi f_{c0}t+\theta_0\right)dt\right)^2\\
&=\sum_{i=0}^{N_c-1}\left(\frac{2}{\pi f_0}\left(\sin\left[\left(i+0.5\right)T_c\cdot\pi f_{c0}+\theta_0\right]\sin\left(\frac{T_c\cdot\pi f_{c0}}{2}\right)\right)\right)^2\\
&=\left(\frac{2\sin\left(\frac{T_c\cdot\pi f_{c0}}{2}\right)}{\pi f_{c0}}\right)^2\sum_{i=0}^{N_c-1}\sin^2\left[\left(i+0.5\right)\pi f_{c0}T_c+\theta_0\right]
\end{aligned}
$$

If:

$$
\varphi_1\left(f_c\right)\triangleq\left(\frac{2\sin\left(\frac{\pi f_{c0}T_c}{2}\right)}{\pi f_{c0}}\right)^2=\left(\frac{2\sin\left(\frac{\pi f_{c0}}{2f_c}\right)}{\pi f_{c0}}\right)^2
$$

$$
\begin{aligned}
\varphi_2\left(f_c\right)&\triangleq\sum_{i=0}^{N_c-1}\sin^2\left(\pi f_{c0}T_c\left(i+0.5\right)+\theta_0\right)\\
&=\sum_{i=0}^{N_c-1}\sin^2\left(\frac{\pi f_{c0}\left(i+0.5\right)}{f_c}+\theta_0\right)
\end{aligned}
$$

Then:

$$
J\left(f_c,0\right)=\varphi_1\left(f_c\right)\cdot\varphi_2\left(f_c\right)
$$

where $\varphi_1\left(f_c\right)$ is a large-scale fluctuation term, and the peak width is determined by the small-scale fluctuation term $\varphi_2\left(f_c\right)$, which can be further derived as follows:

$$
\begin{aligned}
\varphi_2\left(f_c\right)&=\sum_{i=0}^{N_c-1}\sin^2\left(\frac{\pi f_{c0}\left(i+0.5\right)}{f_c}+\theta_0\right)\\
&=\sum_{i=0}^{N_c-1}\frac{1}{2}\left(1-\cos\left(\frac{\left(2i+1\right)\pi f_{c0}}{f_c}+\theta_0\right)\right)\\
&=\frac{N_c}{2}-\frac{1}{2}\sum_{i=0}^{N_c-1}\cos\left(\frac{\left(2i+1\right)\pi f_{c0}}{f_c}+\theta_0\right)
\end{aligned}
$$

In $\frac{N_c}{2}-\frac{1}{2}\sum_{i=0}^{N_c-1}\cos\left(\frac{(2i+1)\pi f_{c0}}{f_c}+\theta_0\right)$, the minimum periodic term of the triangular function determines the peak width, i.e., when $i=N_c-1$ and $\cos\left(\frac{(2N_c-1)\pi f_{c0}}{f_c}+\theta_0\right)$, the Taylor expansion of $\frac{1}{f_c}$ at $f_c=f_{c0}$ is $\frac{1}{f_c}=\frac{1}{f_{c0}}-\frac{1}{f_{c0}^2}\left(f_c-f_{c0}\right)+o\left(\cdot\right)$ and:

$$
\begin{aligned}
&\cos\left(\frac{\left(2N_c-1\right)\pi f_{c0}}{f_c}+\theta_0\right)\\
&=\cos\left(\left(2N_c-1\right)\pi f_{c0}\left(\frac{1}{f_{c0}}-\frac{1}{f_{c0}^2}\left(f_c-f_{c0}\right)+o\left(\cdot\right)\right)+\theta_0\right)
\end{aligned}
$$

Therefore, the fluctuation period near f_{c0} is:

$$
f_{width}=\frac{2\pi f_{c0}}{\left(2N_c-1\right)\pi}\approx\frac{f_{c0}}{N_c}
$$

When $f_c=f_{c0}$, $N_c=T_sf_{c0}$, then: $f_{width}\approx\frac{1}{T_s}$.

REFERENCES

[1] Y. Zhan, Z. Cao, and J. Lu, "Spread-spectrum sequence estimation for DSSS signal in non-cooperative communication systems," *IEE Proc. Commun.*, vol. 152, no. 4, pp. 476–480, Aug. 2005.

[2] H.-C. Hwang and C.-H. Wei, "Adaptive blind demodulation of DS/CDMA signals with transform domain Griffiths' algorithm," in *Proc. IEEE Int. Symp. Circuits Syst.*, May/Jun. 1999, pp. 25–28.

[3] F. M. Gardner, *Phaselock Techniques*, 2nd ed. New York, NY, USA: Wiley, 1979, pp. 73–74.

[4] A. N. D'Andrea, U. Mengali, and R. Reggiannini, "The modified Cramer-Rao bound and its application to synchronization problems," *IEEE Trans. Commun.*, vol. 42, no. 234, pp. 1391–1399, Feb./Mar./Apr. 1994.

[5] A. N. D'Andrea and U. Mengali, *Synchronization Techniques for Digital Receivers* (Applications of Communications Theory). Pisa, Italy: Springer, 1997.

[6] J. W. Betz and K. R. Kolodziejski, "Generalized theory of code tracking with an early-late discriminator part I: Lower bound and coherent processing," *IEEE Trans. Aerosp. Electron. Syst.*, vol. 45, no. 4, pp. 1538–1556, Oct. 2009.

[7] L. Erup, F. M. Gardner, and R. A. Harris, "Interpolation in digital modems. II. Implementation and performance," *IEEE Trans. Commun.*, vol. 41, no. 6, pp. 998–1008, Jun. 1993.

[8] Q. Zhang, W. Gao, and H. Zhao, "A new lock detection algorithm for Gardner's timing recovery," in *Proc. IEEE Int. Conf. Commun. Technol.*, Sep. 2011, pp. 319–322.

[9] F. Gardner, "A BPSK/QPSK timing-error detector for sampled receivers," *IEEE Trans. Commun.*, vol. 34, no. 5, pp. 423–429, May 1986.

[10] B. A. Bhatti, M. Umer, W. Ahmed, M. H. Tariq, and U. Ali, "Carrier and symbol synchronization in digital receivers using feedback compensation loop and early late gate on FPGA," in *Proc. Int. Conf. Robot. Emerg. Allied Technol. Eng.*, Apr. 2014, pp. 146–150.

[11] P. Shachi, R. Mishra, and R. K. Jatoth, "Coherent BPSK demodulator using Costas loop and early-late gate synchronizer," in *Proc. 4th Int. Conf. Comput., Commun. Netw. Technol. (ICCCNT)*, Jul. 2013, pp. 1–6.

[12] D. Kaplan Elliott and J. Hegarty Christopher, *Understanding GPS: Principles and Applications*. Norwood, MA, USA: Artech House, 2006, p. 174.

[13] H. Lou and P. Lin, "A new lock detector for Gardner's timing recovery method," *IEEE Trans. Consum. Electron.*, vol. 54, no. 2, pp. 349–352, May 2008.

[14] W. Leng, Z. Yu, and Z. Yang, "A modified Gardner detector for multi-level PAM/QAM system," in *Proc. Int. Conf. Commun., Circuits Syst.*, May 2008, pp. 891–895.

[15] Gappmair, W. Cioni, S. Corazza, and G. E. Koudelka, "Extended gardner detector for improved symbol-timing recovery of M-PSK signals," *IEEE Trans. Commun.*, vol. 54, no. 11, pp. 1923–1927, Nov. 2006.

[16] K. Shi and E. Serpedin, "Fast timing recovery for linearly and nonlinearly modulated systems," in *Proc. Asilomar Conf. Signals, Syst. Comput.*, Nov. 2004, pp. 1015–1019.

[17] F. Gardner, "Self-noise in synchronizers," *IEEE Trans. Commun.*, vol. COMM-28, no. 8, pp. 1159–1163, Aug. 1980.

[18] F. Scardoni, M. Magarini, and A. Spalvieri, "Impact of self noise on tracking performance of non-data-aided digital timing recovery," *J. Lightw. Technol.*, vol. 33, no. 18, pp. 3755–3762, 2015.

[19] E. R. Pelet and J. E. Salt, "On economical timing-error detectors for QAM receivers," *IET Commun.*, vol. 1, no. 4, pp. 618–622, Aug. 2007.

[20] Y. Ding, L. Zan, J. Si, F. Zhou, and B. Hao, "A self-adapting symbol rate estimator based on wavelet transform with optimal scale and resample," in *Proc. IEEE 80th Veh. Technol. Conf.* , Sep. 2014, pp. 1–5.

[21] G. J. Phukan and P. K. Bora, "An algorithm for blind symbol rate estimation using second order cyclostationarity," in *Proc. Int. Conf. Signal Process. Commun. (SPCOM)*, Jul. 2014, pp. 1–6.

[22] E. R. Pelet and J. E. Salt, "Timing jitter analysis of optimum non-data-aided symbol synchronizer for QAM," *IEEE Trans. Commun.*, vol. 58, no. 4, pp. 1247–1255, Apr. 2010.

[23] M. Oerder and H. Meyr, "Digital filter and square timing recovery," *IEEE Trans. Commun.*, vol. 36, no. 5, pp. 605–612, May 1988.
[24] V. T. Tran, N. C. Shivaramaiah, T. D. Nguyen, E. P. Glennon, and A. G. Dempster, "GNSS receiver implementations to mitigate the effects of commensurate sampling frequencies on DLL code tracking," *GPS Solutions*, vol. 22, no. 1, p. 24, Jan. 2018.

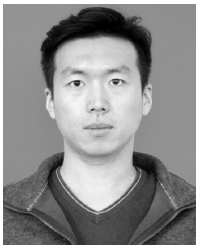

YOUYANG LI received the B.Sc. degree from the Faculty of Mathematics, Northwest University, Xi'an, Shanxi, in 2014. He is currently pursuing the Ph.D. degree in communication and information system with the Navigation and Communication Laboratory, National Time Service Center, Chinese Academy of Sciences. His major interests are in satellite communication signal detection and detection and evaluation of satellite navigation signal, and blind demodulation.

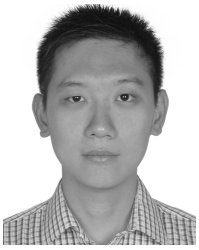

FEI QIN (S'05–M'12) received the B.Eng. degree in information engineering from the Huazhong University of Science and Technology, Wuhan, China, in 2004, the M.Eng. degree in electronic engineering from the Beijing Institute of Technology, Beijing, China, in 2006, and the Ph.D. degree in electronic and electrical engineering from University College London, London, U.K., in 2012.

He is currently an Associate Professor with the School of Electronic and Electrical Communication Engineering, University of Chinese Academy of Sciences, Beijing. Prior to that, he served as a Product Manager with Crossbow Technology, Beijing Representative Office, from 2006 to 2008. His current research interests include the joint optimization method of wireless networks and information systems for industrial applications.

XUE WANG received the master's degree from Xidian University, Xi'an, China, in 2007, and the Ph.D. degree in astrometry and celestial mechanics from National Time Service Center, Chinese Academy of Sciences, Xi'an, China, in 2011. He works as a Research Fellow with the National Time Service Center, Chinese Academy of Sciences. His research interests focus on the time and frequency measurement technology, GNSS signal in space quality assessment, and signal receiving and processing.

XIAOCHUN LU received the Ph.D. degree from the National Time Service Center, Chinese Academy of Sciences, in 2004. She is currently a Researcher, a Ph.D. Tutor, and the Deputy Director of the National Time Service Center, Chinese Academy of Sciences. She is mainly engaged in the design and construction of satellite navigation and positioning system. She is also the Deputy Head of the China Area Positioning System (CAPS) Navigation Group, a major project of knowledge innovation of the Chinese Academy of Sciences. Her research interests include precision time information transmission and information processing, and radio ranging technology and positioning navigation.